Using Stress Intensity Factors in Fracture Load Estimation for IC Ceramic Packages

Ishibashi, Masahiro
Department of Molecular and Material Sciences, Ph. D Student and Nano Electronics Research Laboratories, NEC Corporation

Nakashima, Hideharu
Department of Molecular and Materials Sciences, Kyushu University

Using Stress Intensity Factors in Fracture Load Estimation for IC Ceramic Packages

Masahiro ISHIBASHI[*1] and Hideharu NAKASHIMA[*2,†]

[†]E-mail of corresponding author: *nakasima@mm.kyushu-u.ac.jp*

We have developed a new type of method of estimating fracture loads using stress intensity factors in IC ceramic packages under complicated load conditions. The right-angle corners in the cross sections of IC ceramic packages were assumed to be wedge cracks, and the fracture criterion was defined as curved surface in Mode I (tensile opening)-Mode II (in-plane shear)-Mode III (tearing) coordinate space.

Key words: *Stress intensity factor, Fracture criterion, Crack, IC ceramic package*

1. Introduction

One of the major problems in IC package development is ceramic package cracking, which directly affects IC device reliability. These cracks are most likely to originate along the lines at which layer stacking, during the fabrication process, has formed sharp right-angle corners[1,2]. If fracture load conditions could be predicted by computer-simulation analysis and by simple experimental procedures using specimens without notch and pre-crack, it would be possible to design more reliable IC packages than ever before. To date, many studies have been carried out on the mixed-mode fracture toughness of ceramics materials using stress intensity factors[3-13]. Because of the extremely high stress concentration around the sharp right-angle corners, the fracture load cannot be estimated by using conventional approaches based on maximum principal stress values obtained by finite element analysis. However, although estimates based on mixed-mode stress intensity factors would seem to be a promising alternative, this approach presents two main difficulties: 1) how to apply stress intensity factors to the right-angle corners, and 2) how to evaluate the material's initial resistance to the fractures for each mode.

This paper discusses the fracture criteria for actual IC alumina ceramic packages with right-angle corners. To obtain the criteria, we examined stress intensity factors in alumina samples under a variety of load conditions. The cross sections of alumina ceramic plates were observed by optical and scanning electron microscopy (SEM).

2. Experimental Method

2.1 Bending Specimens

The samples used in this study were composed of fine-grained polycrystalline Al_2O_3 with a 10 μm average grain size. The tensile-opening fracture toughness (K_{Ic}) of this material had been determined by the manufacturer, based on the single edge pre-cracked beam (SEPB) method, to be 3.8 $MPa\sqrt{m}$. Figure 1 shows micrographs of the cross section of an alumina ceramic plate obtained by optical microscopy and SEM. An IC ceramic package is formed by piling plural unsintered alumina sheets called greensheets. As seen in Fig. 1, however, neither borders as the origins of cracks nor heterogeneity can be observed.

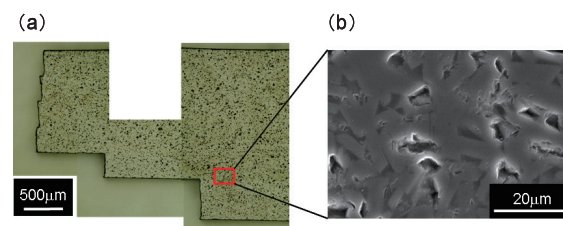As shown in Fig. 2, 4-mm-wide samples were cut from an alumina ceramic plate (40 × 40

Fig.1 Cross section of alumina ceramic plate. (a) Optical microscopy image. (b) Scanning electron microscope image.

*1 Department of Molecular and Material Sciences, Ph. D Student and Nano Electronics Research Laboratories, NEC Corporation
*2 Department of Molecular and Material Sciences

× 2.5 mm) containing a square cavity (15 × 15 × 0.5 mm). We used two sample shapes: the first was cut parallel to the side surface of the plate (Fig. 2(a)) and the second was angled 30° from that surface (Fig. 2(b)). SEM images revealed the radius of curvature for the corners (where the sides of the cavity meet the cavity base) to be approximately 10 µm. None of the samples exhibited any notches or pre-cracks.

2.2 Mixed-Mode Loading Experiment

We conducted three-point bending tests as mixed-mode fracture tests at room temperature (RT) and at a bending speed of 0.1 mm/min, as seen in Fig. 3. The samples for the first (parallel) shape were tested under three different conditions, i.e., location angles (that between the supporting edge and the cavity line) of 0°, 15° and 30°. The samples for the second shape (angled at 30°) were only tested at a location angle of 0°. In the discussion that follows, we will refer to these four tests as Tests A to D. The stress distributions around the cavity corners were expected to differ between the four test cases.

3. Stress Intensity Factors

3.1 Finite Element Analysis

We carried out stress-simulation analysis by using finite element analysis for each bending test on the basis of experimental fracture loads. Young's modulus, used in the stress simulation, was 260 GPa and Poisson's ratio was 0.3. We employed a three-dimensional isoparametric solid element. A typical sample geometry was composed of 3000 elements, with a total of 3927 nodes. Figure 4 shows a finite element mesh for test sample A with a 0.5-mm-deep cavity. The mesh size adjacent to the cavity corner was about 10 µm. We used the CAE software I-DEAS (INCAT International) for the finite element modeling and conducted stress simulation with ANSYS (ANSYS, Inc.) structural solution program.

3.2 Stress Intensity Factors

Figure 5 shows the experimental and analytical fracture-load test results (determined during previous tests) versus the radii of curvatures in the cavity corner for the samples. The test samples were cut from a ceramic IC package plate and subjected to four-point bending tests. The hatched solid lines indicate the fracture loads predicted on the basis of
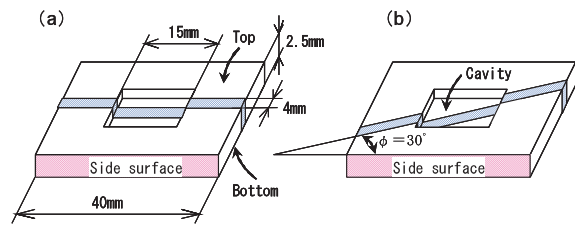
Fig.2　Bending samples cut from IC ceramic plates. (a) Sample cut out parallel to side surface. (b) Sample cut out 30° (ϕ) off same side surface.

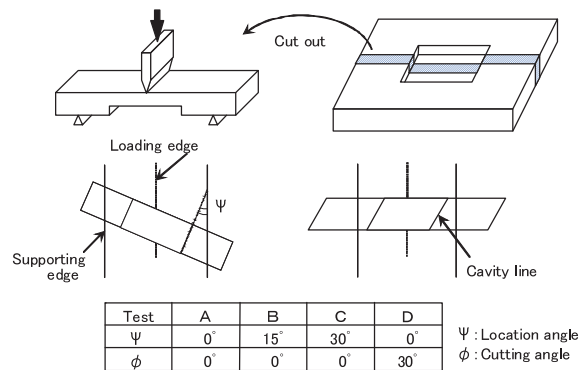| Test	A	B	C	D
Ψ	0°	15°	30°	0°
ϕ	0°	0°	0°	30°

Ψ : Location angle
ϕ : Cutting angle

Fig.3　Three-point bending-test conditions for ceramic samples.
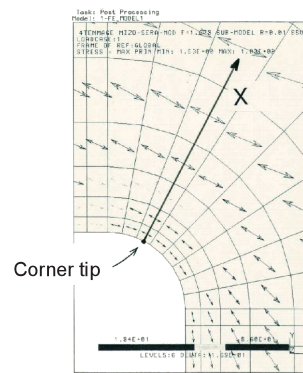
Fig.4　Finite element model for cavity corner in Test A, and direction x for calculating stress intensity factors.

maximum principal stress values after finite element analysis. The curvature radii for the cavity-corner geometries were modeled for individual test samples. Fracture loads were determined on the basis of the tensile strength for the material (300-400 MPa). The open circles in the figure indicate the measured fracture loads and the error bars indicate scattering. Below 50 µm, the experimental measured values become constant irrespective of the curvature radii, and the discrepancy between the predicted fracture load and the measured
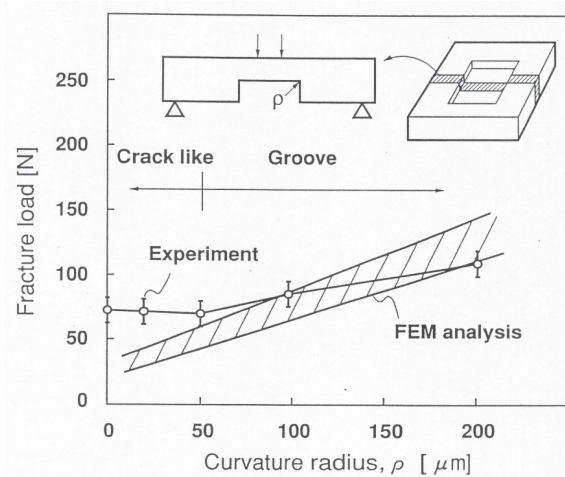
Fig.5 Experimental and analytical fracture loads versus radius of curvature at cavity corner.

load becomes greater as the radii become smaller. These results suggest that the cavity corners act as wedge cracks when the curvature radius is less than 50 μm, and since the radius values of the samples' cavity corners in Tests A-D were only about 10 μm, the corners may be regarded as wedge cracks, as shown in Fig. 6.

When wedge cracks are subjected to far-field stress σ, the stress intensity factor at the corner tip, K, may be given by:

$$K = \sigma(2\pi x)^{\gamma}, \tag{1}$$

where x refers to the distance from the corner tip in the direction of crack propagation, and γ (=1- λ) is the stress singularity order, which is 0.5 for a conventional crack geometry whose opening angle is zero. The σ is the stress. This is σ_y for Mode I (tensile-opening mode), shear stress τ_{xy} for Mode II (in-plane shear mode), and τ_{yz} for Mode III (tearing mode).

The stress singularity orders for the three fracture modes can be calculated from[14,15]:

Mode I : $\lambda_1 \sin(2\alpha) + \sin(2\alpha\lambda_1) = 0$

Mode II : $\lambda_2 \sin(2\alpha) - \sin(2\alpha\lambda_2) = 0$,   (2)

Mode III : $\sin(2\alpha\lambda_3) = 0$

where $\alpha = \pi - \beta$ and opening crack angle 2β is $\pi/2$ for a right-angle wedge crack (see Fig. 6(a)). From the equations in (2), we find λ_1=0.544, λ_2=0.908 and λ_3=0.667 for a right-angle wedge crack (opening crack angle 2β is $\pi/2$). As given below, the stress singularity order values, applied to right-angle corners for individual modes, may be expressed as :

$$\begin{aligned} \gamma_1 &= 1 - \lambda_1 = 0.456 \\ \gamma_2 &= 1 - \lambda_2 = 0.092 \\ \gamma_3 &= 1 - \lambda_3 = 0.333 \end{aligned} \tag{3}$$

Figure 7 plots the calculated stress singularity orders for individual modes versus opening angle 2β. The stress intensity factors of the right-angle corners for the three fracture modes are defined as:

Mode I : $K_I' = \sigma_y(2\pi x)^{0.456}$

Mode II : $K_{II}' = \tau_{xy}(2\pi x)^{0.092}$ (4)

Mode III : $K_{III}' = \tau_{yz}(2\pi x)^{0.333}$

Once the stress component values (σ_y, τ_{xy}, τ_{yz}) and the distance from the corner tip (x) are known from finite element analysis, K_I', K_{II}' and K_{III}' can be calculated with these three equations.
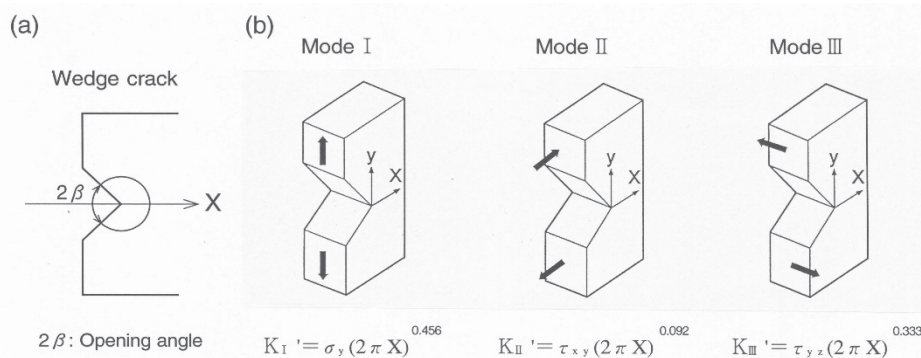

Fig.6 Stress intensity factors for right-angle corner. (a) Opening angle, defined for wedge crack. (b) Stress intensity factors for individual fracture modes.
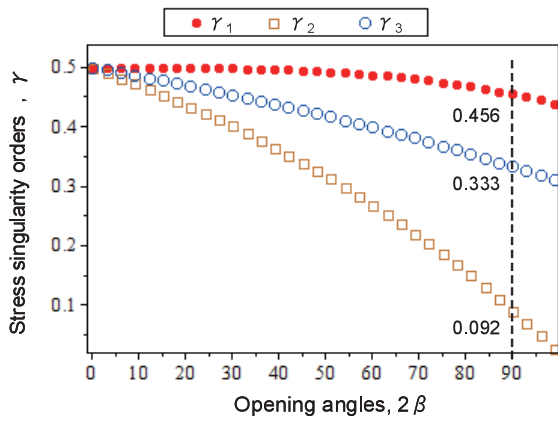
Fig.7 Stress singularity orders of individual modes versus opening angles.
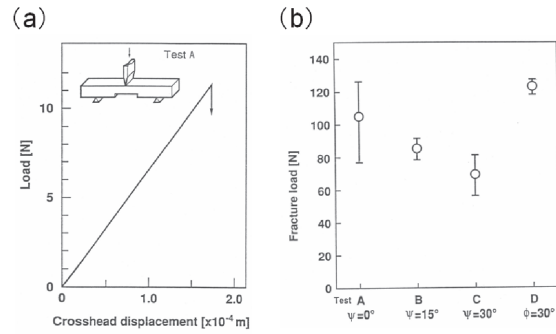

Fig.8 Fracture load in 3-point bending tests. (a) Load-displacement curve in Test A. (b) Fracture loads and their scattering for Tests A-D.

4. Results and Discussion

4.1 Fracture Load

Figure 8(a) shows the load-displacement curve in Test A. The load increases linearly with bending displacement up to the fracture load. The maximum load fracture occurred at the cavity corner tip. The fracture loads for test conditions A-D are presented in Fig. 8(b). Five samples were evaluated for each test. The average fracture load values were 105.0 N (in Test A), 86.3 N (Test B), 69.7 N (Test C) and 123.6 N (Test D) as listed in Table 1. The fracture-load strength decreased as location angle Ψ values increased (Tests A→C). The largest fracture load was observed in Test D.

4.2 Fracture Morphology

The original cracking points and crack initiation paths were confirmed from SEM images for fractured samples. Figure 9 shows fractured surfaces for Tests A, C and D. The fractography indicated that crack origins (indicated here by the solid triangles) occurred near the sides of the samples for Tests A and D. In contrast to this, the crack origin in Test C was observed at the middle of the cavity line. Test B obtained results similar to those for Test C. Figure 10 shows a side view of a fractured sample in Test A. In all Test-A samples, cracks were curved lines, and the initial cracking directions (x) were at angles of approximately 20° from the vertical line; we refer to this angle as crack deflection angle θ. Direction x in Fig. 4 is vertical to the maximum principal-stress direction, obtained from finite element analysis, and deflection angle θ is about 30°. Our experimental results were
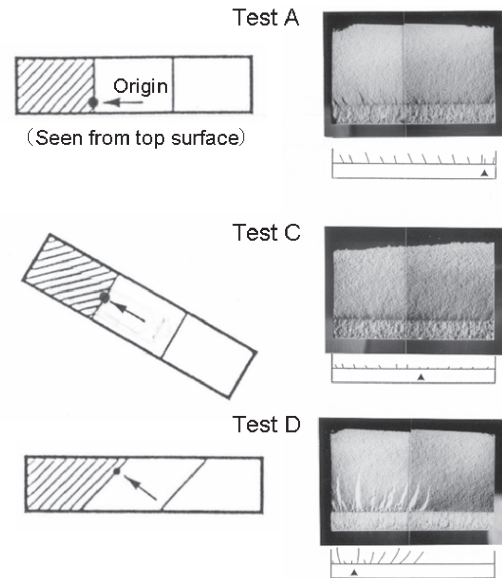

Fig.9 Test cases: Solid circles at left of figure indicate crack origins and arrows represent direction of view for micrographs of fractured surfaces shown at right of figure for Tests A, C and D.
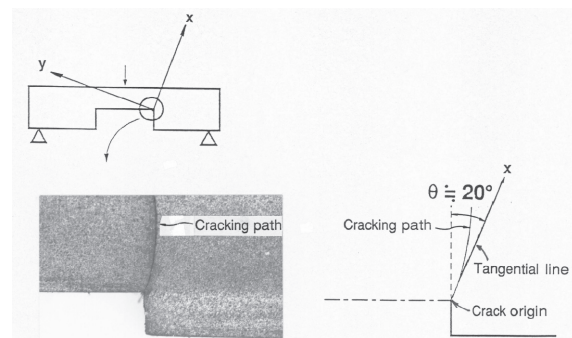

Fig.10 Micrograph is side view of fractured cavity corner of Test A sample. X represents initial cracking direction. θ represents crack deflection angle, which is approximately 20°.

reproduced for all four tests, and were in good agreement with finite element analysis. Stress intensity factors were calculated using both crack tips and initial propagation directions as shown in Fig. 4.

4.3 Stress Intensity Factors

Figure 11 plots the calculated stress intensity factors K_I', K_{II}' and K_{III}' versus the distance from cavity corner tip x for Test C using the equations in (4). In the range shown here, individual calculated points approximately lay along one line, except near the minimum x value. This difference resulted from error produced by the corner mesh geometry. Corner-tip stress intensity factors can be obtained by extrapolation to x=0. These individual extrapolated stress intensity factors are expressed as K_I', K_{II}' and K_{III}' after this. The fracture loads and individual-mode stress intensity factor values for each test are listed in Table 1. The ratios for K_I', K_{II}' and K_{III}' differ in all four bending tests. The Mode III fracture stress intensity factor K_{III}' values range from 0.2 to 0.65 MPa·m$^{0.333}$.

4.4 Mixed-Mode Fracture Criteria

This section discusses, on the basis of the above results, the fracture criteria for a right-angle corner geometry under mixed-mode loading conditions.

4.4.1 Criteria Using Stress Intensity Factors for Three Modes

Figure 12 shows the calculated Mode I stress intensity factor K_I' values under fracture load for individual tests. The open circles in the figure denote the average K_I' values for five fracture-load measurements. These average values ranged widely from 1.9 (Test B) to 3.8 MPa·m$^{0.456}$ (Test D). It appears that the fracture criterion cannot definitely be determined from the K_I' value alone. In the same way, the average values for K_{II}' and K_{III}' ranged widely in each test. These results seem to indicate that no fracture criterion existed in any of the three modes.

Further, the tensile-opening crack fracture toughness of this material, K_{Ic} (=3.8 MPa $\sqrt{m}$), could not be employed as a fracture criterion for a right-angle corner geometry.

4.4.2 Fracture Criteria for Conventional Crack Geometry

A number of theories have been advanced for conventional crack geometry (opening angle 2β=0) to predict fracture under mixed-mode conditions. Awaji and Sato calculated the individual-mode fracture toughness K_{Ic}, K_{IIc} and K_{IIIc} values using inclined large cracks in diametral compression for graphite, plaster and marble materials[16]. They expressed the mixed-mode fracture criterion for marble in terms of a circular curved surface form as:

$$\left(\frac{K_I}{K_{Ic}} \right)^2 + \left(\frac{K_{II}}{K_{IIc}} \right)^2 = 1 \qquad (5)$$
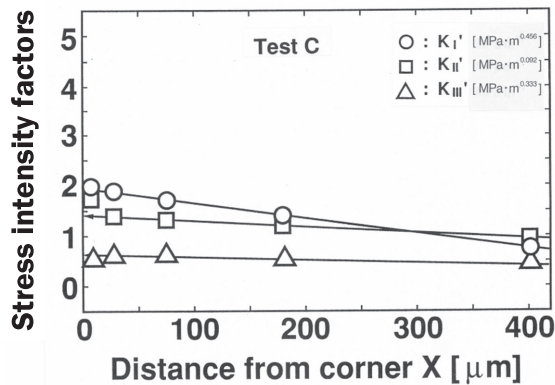

Fig.11 Individual-mode stress intensity factors versus distance from corner tip, obtained by extrapolation to x=0.

Table 1 Fracture loads and individual-mode stress intensity factor values under those loads.

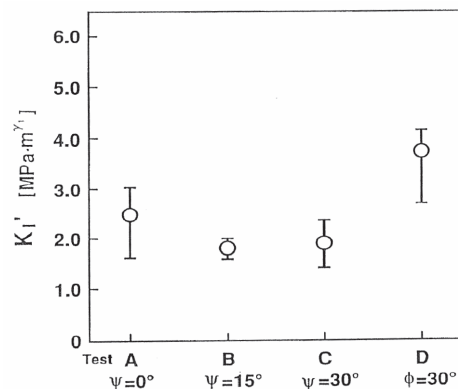|	Test A	Test B	Test C	Test D	Mode I test
Fracture load [N]	105.0	86.3	69.7	123.6	122.1
K_I' [MPa·m$^{0.456}$]	2.5	1.9	2.0	3.8	4.6
K_{II}' [MPa·m$^{0.092}$]	2.2	1.6	1.5	2.9	0
K_{III}' [MPa·m$^{0.333}$]	0.2	0.65	0.6	0.4	0

Fig.12 Calculated stress intensity factor K I ' values under individual fracture loads.

The measured data for the graphite and plaster were on the following curve:

$$\left(\frac{K_{\mathrm{I}}}{K_{\mathrm{I}c}}\right)^{1.6} + \left(\frac{K_{\mathrm{II}}}{K_{\mathrm{II}c}}\right)^{1.6} = 1 \qquad (6)$$

In Petrovic's[17] and Petrovic and Mendiratta's[18] examination of mixed-mode fractures in notched samples of hot-pressed Si₃N₄, the experimental values for K_{I}–K_{II} fractures in slotted-tubes agreed closely with

$$\left(\frac{K_{\mathrm{I}}}{K_{\mathrm{I}c}}\right)^{1.5} + \left(\frac{K_{\mathrm{II}}}{K_{\mathrm{II}c}}\right)^{1.5} = 1 \qquad (7)$$

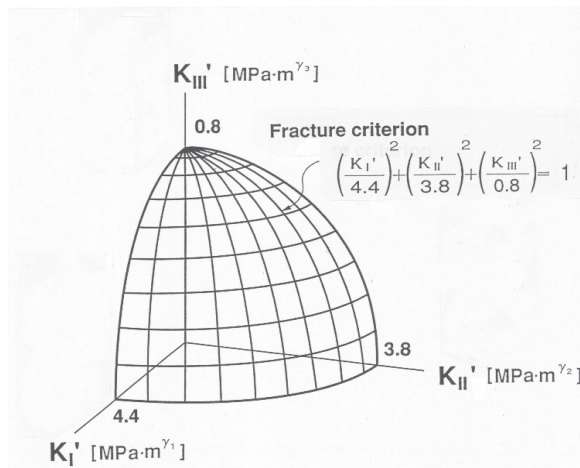while those for K_{I}–K_{III} fractures in notched-rods agreed closely with

Fig.13 Fracture criterion as enveloping curved surface, defined from measurements under mixed-mode fracture conditions.

$$\left(\frac{K_{\mathrm{I}}}{K_{\mathrm{I}c}}\right)^{1.5} + \left(\frac{K_{\mathrm{III}}}{K_{\mathrm{III}c}}\right)^{1.5} = 1 \qquad (8)$$

In these studies, pure-mode fracture toughness values $K_{\mathrm{I}c}$, $K_{\mathrm{II}c}$ and $K_{\mathrm{III}c}$ were measured experimentally, and an exponent was selected from experimental data to define the mixed-mode fracture criterion.

In Suresh's et al.[19-21] examination of mixed-mode fractures in sharp pre-crack samples of polycrystalline Al₂O₃, the pure torsional fracture-toughness $K_{\mathrm{III}c}$ was 2 to 3 times greater than $K_{\mathrm{I}c}$.

4.4.3 Fracture Criterion for Right-Angle Corners

We assume here, as has been done in the previous studies, that we can obtain a mixed-mode fracture criterion for right-angle corners by normalizing for all fracture toughness values, and we extend this concept to a three-dimensional mode. For right-angle corners in an IC ceramic package, stress singularity orders for individual fracture modes differ, and none of them corresponds to the 0.5 of a conventional crack. We assume a mixed-mode fracture criterion for right-angle corners can be expressed as:

$$\left(\frac{K_{\mathrm{I}}'}{K_{\mathrm{I}c}'}\right)^{2} + \left(\frac{K_{\mathrm{II}}'}{K_{\mathrm{II}c}'}\right)^{2} + \left(\frac{K_{\mathrm{III}}'}{K_{\mathrm{III}c}'}\right)^{2} = 1 \qquad (9)$$

The equation represents an enveloping curved surface in K_{I}'–K_{II}'–K_{III}' space, as presented in Fig. 13. Because the pure-mode fracture toughness for right-angle corner geometries is often difficult to measure, we chose
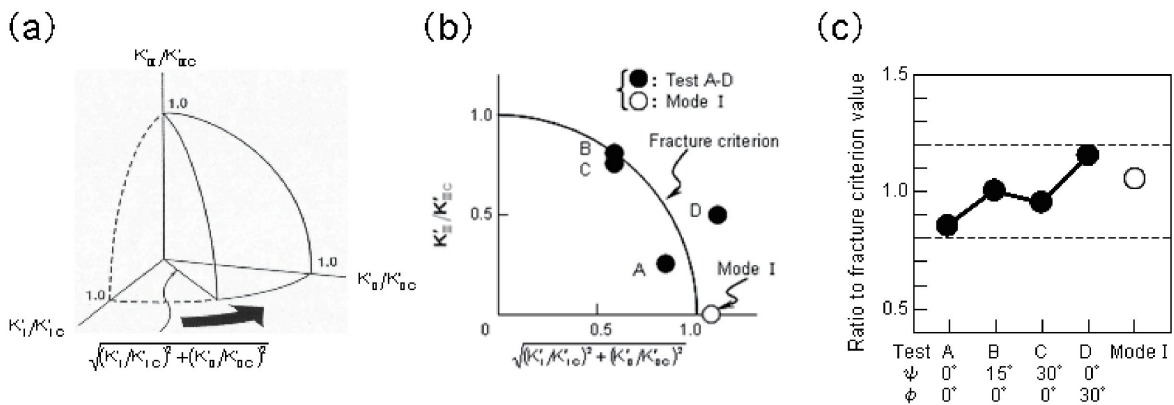

Fig.14 Fracture criterion compared with individual test data. (a) Normalization with individual-mode fracture-toughness values. (b) Superimposed fracture criterion. (c) Normalized values of stress intensity factors.

the approach of selecting K_{Ic}', K_{IIc}' and K_{IIIc}' values, which makes the surface fit the data listed in Table 1 for experimental Tests A-D. In this case, K_{Ic}'=4.4 MPa·m$^{0.456}$, K_{IIc}'=3.8 MPa·m$^{0.092}$ and K_{IIIc}'=0.8 MPa·m$^{0.333}$. In this way, we are able to establish the criterion more easily than if we had to depend on measured values. The calculated K_{Ic}', K_{IIc}' and K_{IIIc}' represent individual pure-mode fracture-toughness values.

The K_I', K_{II}' and K_{III}' in Fig. 13 were normalized with K_{Ic}', K_{IIc}' and K_{IIIc}'. The K_I'/K_{Ic}' axis was superimposed on the K_{II}'/K_{IIc}' axis, as shown in Fig. 14(a). Figure 14(b) compares the fracture criterion with individual test data, represented by the closed circles. The fracture criterion curve was drawn to fit the data for Tests A-D. As shown in Fig. 14(c), all the data fit the fracture criterion within a reasonable experimental error range.

In addition to Tests A-D, an identification sample made from the same material was also tested under four-point bending conditions to determine pure Mode I fracture toughness for the right-angle corners. Figure 15 shows bending-experiment conditions and a finite element model of the area around the corners. The radius of curvature for this sample was similar to that for Tests A-D. The mesh size of the finite element model was similar to that for the tests. The fracture loads were 118.5-125.0 N, and the average value was 122.1 N in the test. The K_I' value obtained from finite element analysis and extrapolation was 4.6 MPa·m$^{0.456}$, as listed in Table 1. As indicated by the open circles in Figs. 14(b) and (c), this value is similar to the K_{Ic}' (=4.4 MPa·m$^{0.456}$) determined by Eq. (9), which indicates that the fracture criterion illustrated in Fig. 13 is reasonable for a right-angle cavity corner under mixed-mode conditions.

4.5 Fracture load Estimation

We applied the fracture criterion illustrated as an enveloping curved surface in Fig. 13 to predict the fracture load in an actual IC alumina ceramic package. Figure 16(a) shows how the bending test was applied on a carrier stand, and also depicts a finite element mesh modeled from an observed cavity-corner geometry for PGA (Pin Grid Array) packages. The x-axis (the arrow in this figure) indicates the direction the initial crack propagated as determined from the analytical maximum principal-stress direction. With finite element analysis under a unit load, we were able to plot individual-mode stress intensity factors versus distance x. The individual-mode stress intensity factors for the right-angle corner tip were determined by extrapolation to x=0. As a result, we found K_{Ic}'=0.96 MPa·m$^{0.456}$, K_{IIc}'=0 and K_{IIIc}'=0.61 MPa·m$^{0.333}$ under a unit load (981 N).
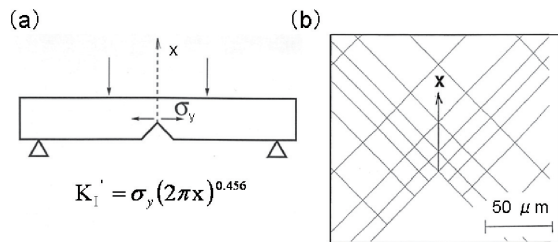

Fig.15 Identification test for right-angle corner under pure mode I fracture loading. (a) Bending experiment conditions. (b) Finite element model of area near cavity corner.
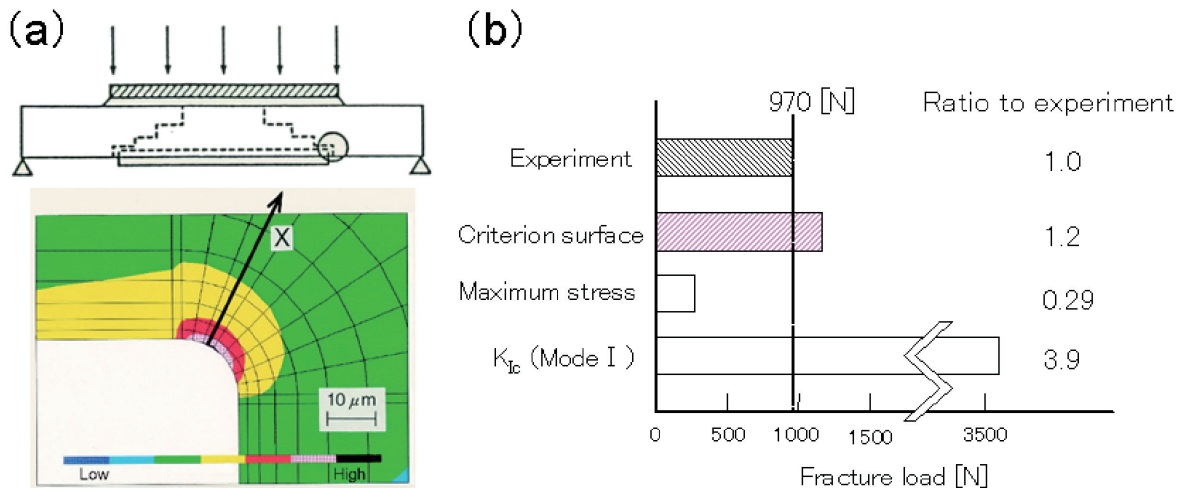
$$K_I' = \sigma_y(2\pi x)^{0.456}$$

Fig.16 PGA package application. (a) Bending-strength test and finite element model of area near cavity corner. (b) Fracture loads estimated from individual criteria.

Using the fracture-criterion curved surface, the fracture load in the PGA package was predicted to be 1200 N. For purposes of comparison, we also made a prediction based on the conventional-crack (opening angle $2\beta = 0$) fracture-toughness value K_{Ic} (3.8 $MPa\sqrt{m}$), and the result was a fracture load value of 3800 N. The fracture load estimated by maximum principal stress value was 280 N. The experimentally determined fracture load for this package was approximately 970 N. The ratio of predicted load to experimentally determined fracture load for each of the two predictions can be seen in Fig. 16(b).

The fracture criterion expressed as the enveloping curved surface defined by Eq.(9) makes it possible to evaluate a fracture load for a PGA package more accurately than that which can be obtained using the conventional criterion.

5.　Conclusions

We considered right-angle corners to be wedge cracks. We used a method of extrapolating stress to obtain, based on finite element analysis, the stress intensity factors for such corners. The stress singularity orders used were 0.456 (for K_I'), 0.092 (K_{II}') and 0.333 (K_{III}'). A mixed-mode fracture-criterion surface in K_I'-K_{II}'-K_{III}' space was easily determined on the basis of mixed-mode loaded bending test data. The fracture criterion demonstrated itself to be capable of enabling the fracture load of actual PGA ceramic packages to be estimated with excellent accuracy.

Acknowledgments

References

1) A. Nishimura, A. Tatemichi, H. Miura and T. Sakamoto: Life Estimation for IC Plastic Packages Under Temperature Cycling Based on Fracture Mechanics, IEEE Trans. on Components, Hybrids and Manufacturing Technology, 1987, pp. 637-642.

2) Y. M. Kasem and L. G. Feinstein: Horizontal Die Cracking as a Yield and Reliability Problem in Integrated Circuit Devices, IEEE Trans. Components, Hybrids, Manuf. Technol., CHMT-12, 1984, pp.

654-661.

3) D. Singh and D. K. Shetty: Fracture Toughness of Polycrystalline Ceramics in Combined Mode I and Mode II Loading, J. Am. Ceram. Soc., 72, 1989, pp. 78-84.

4) D. Singh and D. K. Shetty: Subcritical Crack Growth in Soda-Lime Glass in Combined Mode I and Mode II Loading, J. Am. Ceram. Soc., 73, 1990, pp. 3597-3606.

5) P. C. Paris and G. C. Sih: Fracture Toughness Testing and Its Applications, Am. Soc. Test. Mater., Spec. Tech. Publ., 381, 1965, pp. 30-81.

6) F. Erdogan and G. C. Sih: On the Crack Extension in Plates Under Plane Loading and Transverse Shear, J. Basic Eng., Trans. ASME, 85, 1963, pp. 519-527.

7) S. W. Freiman, A. C. Gonzalez and J. J. Mecholsky: Mixed-Mode Fracture in Soda-Lime Glass, J. Am. Ceram. Soc., 62, 1979, pp. 206-208.

8) D. K. Shetty, A. R. Rosenfield and W. H. Duckworth: Mixed-Mode Fracture of Ceramics in Diametral Compression, J. Am. Ceram. Soc., 69, 1986, pp. 437-443.

9) J. J. Petrovic and M. G. Stout: Fracture of Al_2O_3 in Combined Tension / Torsion: I, Experiments, J. Am. Ceram. Soc., 64, 1981, pp. 656-660.

10) M. G. Stout and J. J. Petrovic: Multiaxial Loading Fracture of Al_2O_3 Tubes: I, Experiments, J. Am. Ceram. Soc., 67, 1984, pp. 14-18.

11) J. J. Petrovic: Effect of Indenter Geometry on Controlled-Surface-Flaw Fracture Toughness, J. Am. Ceram. Soc., 66, 1983, pp. 277-283.

12) D. B. Marshall: Mechanism of Failure from Surface Flaws in Mixed-Mode Loading, J. Am. Ceram. Soc., 67, 1984, pp. 110-116.

13) D. A. Tossell and K. H. G. Ashbee: Measurement of Crack Tip Displacement Fields in Mode I-Mode III Fracture, J. Am. Ceram. Soc., 71, 1988, pp. C138-C144.

14) S. P. Timoshenko and J. N. Goodier: Theory of Elasticity, McGraw-Hill, New York, 1970, pp. 141-144.

15) Williams M. L.: Stress Singularities Resulting from Various Boundary Conditions in Angular Corners of Plates in Extension, Trans. ASME, 74, 1952, pp. 526-528.

16) H. Awaji and S. Sato: Combined Mode Fracture Toughness Measurement by the Disk Test, Trans. ASME, J. Eng. Mater. & Technol., 100, 1978, pp. 175-182.

17) J. J. Petrovic: Mixed-Mode Fracture of Hot-Pressed Si_3N_4, J. Am. Ceram. Soc., 68, 1985, pp. 348-355.

18) J. J. Petrovic and M. G. Mendiratta: Mixed-Mode Fracture from Controlled Surface Flaw in Hot-Pressed Si_3N_4, J. Am. Ceram. Soc., 59, 1976, pp. 163-167.

19) S. Suresh, C. F. Shih, A. Morrone and N. P. O'Dowd: Mixed-Mode Fracture Toughness of Ceramic Materials, J. Am. Ceram. Soc., 73, 1990, pp. 1257-1267.

20) S. Suresh and E. K. Tschegg: Combined Mode I-Mode III Fracture of Fatigue-Precracked Alumina, J. Am. Ceram. Soc., 70, 1987, pp. 726-733.

21) E. K. Tschegg and S. Suresh: Tensile Fracture Toughness Measurements in Ceramics, J. Am. Ceram. Soc., 70, 1987, pp. C41-C43.